Investigation of the Current of P3HT: PCBM-Based Organic Solar Cell Extracting the Spatial Recombination Coefficient of the Active Layer

MD. SHOFIQUL ISLAM

Department of Electrical and Computer Engineering, Faculty of Engineering, King Abdulaziz University, Jeddah 21589, Saudi Arabia

e-mail: msislam@kau.edu.sa; shofiq1992@gmail.com

ABSTRACT The current of P3HT:PCBM-based organic solar cells was analytically investigated in this work. Position-and wavelength-dependent excitons generated by light were evaluated using the optical transfer matrix method. The charge carriers generated by dissociating excitons were estimated using an improved dissociation probability, incorporating a Gaussian distribution. A universal analytical equation was derived by solving the transport equation to calculate the current-producing holes and electrons. Similarly, another universal equation was derived to calculate the hole and electron currents. The total current, calculated using a constant recombination coefficient, is found to be different at different positions (position dependent), which is inconsistent because the total current should be position independent. The use of a constant recombination coefficient is the reason for this inconsistent result. The spatial recombination coefficients inside the active layer were extracted and used in the calculation, and the total current was found to be position independent; thus, the inconsistency was resolved. The current and its components have been investigated with respect to position, terminal voltage, solar irradiance, active layer thickness and wavelength. This work provides better results because it includes spatial recombination coefficients, space-and wavelength-dependent excitons, and improved dissociation probability in analytical calculations; therefore, it will help improve the prediction and design of organic solar cells.

INDEX TERMS P3HT: PCBM-based organic solar cell, investigation of current with spatial recombination coefficients, excitons by optical transfer matrix method, dissociation probability with Gaussian distribution.

I. INTRODUCTION

Organic solar cells (OSCs) have good prospects for harvesting solar energy. Many people [1]–[5] are working on OSCs, assuming it to be an alternative to Si solar cells. The OSC research is attracting the attention of researchers because the chemical structure of organic materials can be modified, large solar panels can be easily made, organic materials are cheaper, and organic materials are lightweight. Basically, OSC is a layered device; one layer works to absorb incident light (photons), which is known as the active layer; the other layers work as a contact layer, guiding layer, or supporting

layer. The active layer is made of two materials: one (P3HT) donates electrons and the other (PCBM) accepts electrons.

The incident light generates excitons (tightly bound electron-hole pairs) inside the active layer of the OSC. Afterwards, the excitons are dissociated, resulting in free electrons and holes; the free electrons move from donor (P3HT) to acceptor (PCBM), and then they are guided by other layers toward the cathode terminal. Free holes move from PCBM to P3HT and are guided by other layers toward the anode terminal. While the excitons interact with any defect states or with the interface of P3HT and PCBM, the excitons dissociate; however, the interface plays the main role of dissociation because the interface possesses an electric field. If P3HT and PCBM are distinctly separate layers, then there will be a single interface, the excitons generated near this single

The associate editor coordinating the review of this manuscript and approving it for publication was Stavros Souravlas.

interface will be dissociated, and the excitons that are far away from that single interface vanish (electrons fall into holes of the same exciton) before reaching the interface; therefore, the efficiency is not good. Instead, if P3HT and PCBM are mixed to make an active layer, there will be many interfaces inside the entire active layer, which is known as bulk heterojunction OSC; wherever the excitons are generated, almost every exciton will get a neighboring interface. As a result, the dissociation of excitons increases, and the efficiency increases. Hence, many researchers [6]–[8] are working with bulk heterojunction OSCs.

For a solar cell, the current is the most important because it is an indicator of other performances; therefore, the investigation of current demands special attention. In this work, current investigations were carried out on bulk heterojunction OSCs. In this area, some are working with materials, and some are working with device design for the improvement of OSC because the performance (efficiency) is still not up to the mark. To obtain OSCs with better performance, a theoretical investigation might be carried out to determine suitable materials and/or suitable device structures for the fabrication of OSCs; that is, the theoretical work plays a significant role. Some research groups [9]–[12] have carried out theoretical works with numerical calculations, while others [13]–[16] have used the analytical approach. In this work, an analytical investigation of the OSC current was carried out in detail, considering the effects of different factors. The accuracy of analytical computation depends on the following factors: selection of a suitable function to calculate generated excitons, use of appropriate dissociation probability of excitons to estimate charge carriers, and consideration of recombination.

Some researchers [15] used the constant charge carrier generation rate, which is the simplest approximation, which makes calculations easier. However, naturally, the light intensity (hence excitons, charge carriers) would be different at different positions inside the device. Some researchers considered position dependence by assuming that the light intensity exponentially decreases with position away from the point of incidence. For a single thick (wider) layer, an exponentially decreasing concept may work. But for thin layered device like OSC, while the light passes through a thin layer, it reaches to other side without decreasing much and then it is reflected at the interface, after that the reflected light will interfere with the incident light, we know, light has a wave-like nature, somewhere they will meet in-phase and hence produce high intensity; somewhere they will meet out-of-phase and hence produce low intensity; therefore, the light intensity will have ups and downs at places; as a result, the excitons and charge carriers will have pulsating pattern with positions. This indicates that the exponentially decreasing concept does not consider optical activities (reflection and interference), and hence is not suitable for thin-layered devices. Again, the generation of charge carriers depends on the material that selects the photons (wavelengths) to be absorbed. The optical transfer matrix method (OTMM) includes optical activities and material properties, and hence

calculates position-and wavelength-dependent excitons for thin-layered devices [5], [12], [17], [18]. In this study, the analytical expression derived from the OTMM was used to estimate the exciton generation rate.

Some works [15], [19]–[21] neglected recombination in their calculations; this makes their calculations easier; however, those works fail to analyze devices with recombination. Some other works [22], [23] included recombination in their calculations, but their generation rate was either constant or exponentially decreasing. In this work, recombination was considered in addition to the space-and wavelength-dependent exciton generation rate obtained by OTMM.

For the dissociation probability of excitons, some [9], [12], [24], [25] used the Braun model; others [22], [26] used Wojcik's formula; both models calculate the dissociation probability using the same (constant) separation distance for all excitons. However, naturally, separation distances would be different for different excitons; to include this fact, Gaussian distribution has been incorporated in computing dissociation probability in this work.

While current is calculated using space-and wavelength-dependent generation rate and constant recombination rate (same recombination at all positions inside the active layer), the total current is found to be different at different positions (that is, position dependent), which is inconsistent because the total current of a device should be the same at all positions (that is, position independent). No work has yet been presented to resolve the problem of the position dependency of the total current. Some work [27] presented the current at a certain position and compared it with the experimental value. Some others [26], [28], [29] used the average value of the current to match the experimental results. On the other hand, the literature [30] shows that while the current was calculated using the space-and wavelength-dependent generation rate but neglecting recombination, the current became independent of position. Therefore, it may be assumed that using an incorrect recombination rate is the root cause of the position dependency of the total current. That is, a constant recombination rate was not appropriate. Because of the interaction between forward and reflected light, the intensity of light and hence charge carriers (electrons and holes) are different at different positions; again, recombination depends on the population of electrons and holes; therefore, recombination would be different at different positions.

The recombination rate $(s^{-1}m^{-3})$ is the product of the recombination coefficient (s^{-1}) and the volume density of electrons and holes (m^{-3}). Usually, the current is calculated using the average volume density of the electrons and holes. The average volume density represents the constant density throughout the volume; hence, the recombination coefficient needs to be different at different positions inside the active layer to achieve different recombination rates at different positions. That is, we need to use the positional (spatial) values of the recombination coefficient in the calculation of the OSC current. To date, no work has been reported on calculating the OSC current using the spatial values of the

recombination coefficient. In this study, the spatial recombination coefficient was extracted and used to calculate the OSC current.

This study aims to (i) extract the spatial recombination coefficient inside the active layer of OSC; (ii) evaluate the OSC current using the spatial recombination coefficient to resolve the inconsistency regarding the space invariance property of the total current; (iii) derive and use a universal analytical equation for evaluating both holes and electrons; (iv) use improved analytical calculations that include spatial recombination coefficient, space-and wavelength-dependent excitons, improved dissociation probability incorporating Gaussian distribution, and (v) analyze OSC current and its components with position, terminal voltage, solar irradiance, active layer thickness, and wavelength by improved analytical calculations.

II. EXCITON GENERATION RATE

Excitons are generated by light absorbed in the active layer of an organic solar cell (OSC). The optical transfer matrix method (OTMM) provides the correct profile of generated excitons for thin-layer devices such as OSC [5], [12], [17], [18]. Now, let us look at a short description of OTMM and the analytical equation derived from OTMM for calculating the generated excitons. The details of OTMM have been described in a previous report [31].

When light crosses the interface of two layers, light is reflected and refracted, and the velocity changes, which can be accounted for by the refractive index (η) of the layer materials. Again, while crossing a layer, light is absorbed and light intensity is reduced, which can be accounted for by the extinction coefficient (κ) of the materials. The complex refractive index ($\tilde{\eta}$), which is defined as $\tilde{\eta} = \eta + i\kappa$, includes both η and κ and hence covers the optical phenomena (reflection, refraction, absorption). OTMM first calculates interface matrices and layer matrices using $\tilde{\eta}$; then forms a transfer matrix (scattering matrix) using these interface and layer matrices, then calculates different optical properties using this transfer matrix, and finally calculates the exciton generation rate.

In general, the interface matrix (I_{ab}), corresponding to the interface of two adjacent layers a and b, is defined as follows [12]:

$$I_{ab} = \begin{bmatrix} \dfrac{\tilde{\eta}_a + \tilde{\eta}_b}{2\tilde{\eta}_a} & \dfrac{\tilde{\eta}_a - \tilde{\eta}_b}{2\tilde{\eta}_a} \\ \dfrac{\tilde{\eta}_a - \tilde{\eta}_b}{2\tilde{\eta}_a} & \dfrac{\tilde{\eta}_a + \tilde{\eta}_b}{2\tilde{\eta}_a} \end{bmatrix} \quad (1)$$

where $\tilde{\eta}_a$, $\tilde{\eta}_b$ are complex refractive indices.

The layer matrix (L_c) corresponding to layer c is defined as [12]:

$$L_c = \begin{bmatrix} exp(-i\xi_c d_c) & 0 \\ 0 & exp(i\xi_c d_c) \end{bmatrix} \quad (2)$$

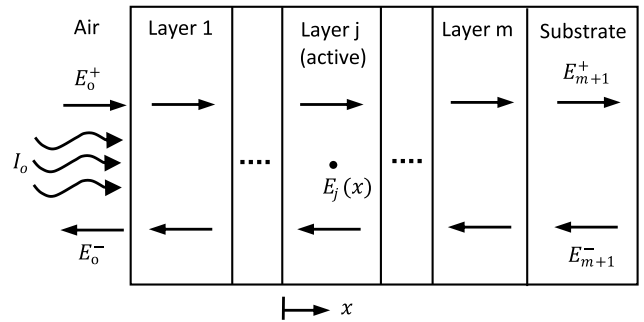where $\xi_c = 2\pi\tilde{\eta}_c/\lambda$; d_c = thickness (width) of layer c.

FIGURE 1. A device of m-layers of different materials with light incident at one side and substrate at another side.

Let us consider an m-layer device (1, 2, 3, ...m) as shown in Fig. 1. Light is incident from the air on one side, and a substrate is placed on the other side as a mechanical support for the thin layers. Air is considered to be the 0th layer, and the substrate to be the $(m + 1)^{th}$ layer.

Calculating all interface and layer matrices, a (2×2) transfer matrix (S) for the entire structure is defined as

$$S = I_{01}L_1I_{12}L_2 \ldots\ldots\ldots\ldots L_mI_{m(m+1)} \quad (3)$$

Because excitons are generated inside the active layer (j^{th} layer), to obtain the exciton profile, we must consider the active layer matrix (L_j), separately. Therefore, the entire transfer matrix (S) may be expressed as $S = S'L_jS''$. Here, S' and S'' are two (2×2) sub-matrices formed with the interface and layer matrices before and after the active layer, respectively, as follows:

$$S' = I_{01}L_1I_{12}L_2 \ldots\ldots L_{(j-1)}I_{(j-1)j} \quad (4)$$
$$S'' = I_{j(j+1)}L_{(j+1)} \ldots\ldots L_mI_{m(m+1)} \quad (5)$$

Each matrix S, S', S'' may be used to relate optical electric fields at its two sides, after algebraic manipulation of these relations, at any position (x) inside active layer, the optical electric field $E_j(x)$ may be determined; the square of the magnitude of $E_j(x)$ is as follows [31].

$$\left| E_j(x) \right|^2 = \left| t_j^+ \right|^2 \left| E_0^+ \right|^2 H(x) \quad (6)$$

The definitions of parameters of Eq. (6) are given in Appendix A.

Irradiance (I) is the power per unit area (unit: Wm^{-2} or $Js^{-1}m^{-2}$). We know [31] that the irradiance equation is $I = (1/2)c\varepsilon E^2$; for incident irradiance, $I_0 = (1/2)c_0\varepsilon_0\left| E_0^+ \right|^2$. Now, the Eq. (6) can be rewritten as:

$$\left| E_j(x) \right|^2 = \left| t_j^+ \right|^2 \frac{2I_0}{c_0\varepsilon_0} H(x) \quad (7)$$

The irradiance at any position (x) inside the active layer is $I_j(x) = (1/2)c_j\varepsilon_j\left| E_j(x) \right|^2$. Using Eq. (7) and the relation between the refractive index (η_j) and electric permittivity (ε_j), the final form of $I_j(x)$ can be obtained as follows [31]:

$$I_j(x) = \frac{\eta_j}{\eta_0}\left| t_j^+ \right|^2 I_0 H(x) \quad (8)$$

If we multiply irradiance $I_j(x)$ [unit: $Js^{-1}m^{-2}$] with absorption coefficient α_j [unit: m^{-1}] and then divide by photon energy (hc/λ) [unit: J], we can obtain the photon incident rate [unit: $s^{-1}m^{-3}$]. Assuming that each photon produces each exciton, we can obtain the exciton generation rate using the following equation [31]:

$$G_{exc}(x) = \frac{\lambda}{hc}\alpha_j\frac{\eta_j}{\eta_0}\left|t_j^+\right|^2 I_0 H(x) \qquad (9)$$

Here, h = Planck's constant; c = light speed.

G_{exc} is a function of position and wavelength. Eq. (9) determines the exciton generation rate for a single wavelength. The exciton generation rate at any position for all the lights can be determined by integrating over the wavelength range.

III. CHARGE CARRIER GENERATION RAT

All of the generated excitons do not dissociate into free charge carriers; however, many of them do. The Onsager theory [24] is useful for calculating the dissociation probability of excitons. However, the Onsager theory cannot describe the exciton behavior at high electric fields [32], [33]. Braun [25] corrected and defined the dissociation probability P as

$$P = \frac{k_{diss}}{k_{diss}+k_f} = \frac{1}{1+(k_f/k_{diss})} \qquad (10)$$

where k_f = decay rate = S_r/r_0; S_r = reactivity parameter (unit: ms^{-1}), r_0 = electron-hole separation distance of the exciton. k_{diss} = dissociation rate; k_{diss} depends on the electric field (F) working across the active layer.

Based on Onsager [34], Braun provided an equation for k_{diss} that has been used in many studies [9], [12], [35]. However, Wojcik's group [30] provided an improved formula for k_{diss} as follows:

$$k_{diss\_W} = \frac{Dr_c}{r_0^3}e^{-\frac{r_c}{r_0}}\left(1+b+\frac{b^2}{3}+\frac{b^3}{18}+\cdots\right) \qquad (11)$$

The definitions of parameters of Eq. (11) are given in Appendix B.

Many researchers [22], [25], [26], [32] have used constant separation-distance (r_0) but naturally different excitons have different separation distances; therefore, a statistical distribution function may be used to address this fact. In this work, the separation distance was considered as variable (r), and the spherically averaged Gaussian distribution (SAGD) function was used along with k_{diss} provided by Wojcik *et al.*; thus, an improved dissociation probability (P) was calculated as follows.

$$P = \int_0^\infty \frac{k_{diss}(r)}{k_{diss}(r)+k_f(r)}f(r)\,dr \qquad (12)$$

where $f(r)$ is the SAGD function given by

$$f(r) = \frac{4}{\sqrt{\pi}r_a^3}r^2 e^{-\frac{r^2}{r_a^2}} \qquad (13)$$

where r = variable separation distance, r_a = the value of r at which the SAGD function value is maximum.
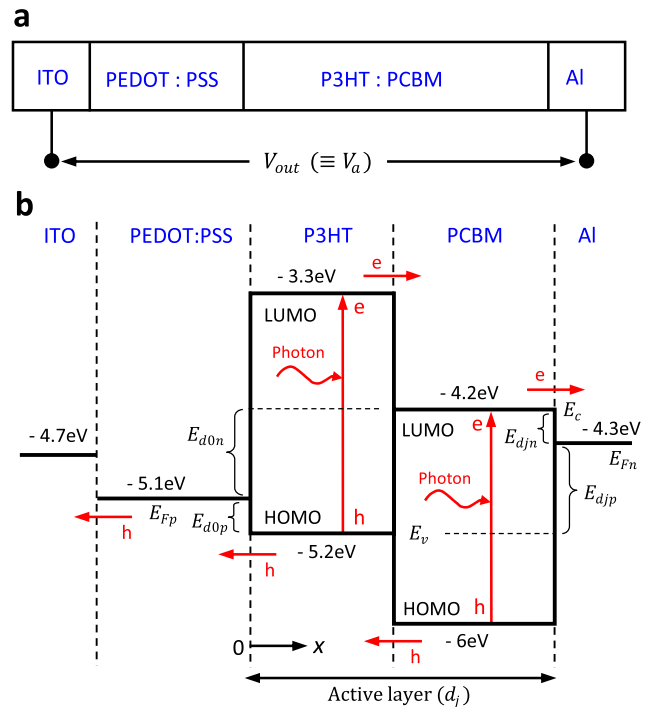

FIGURE 2. (a) P3HT:PCBM based OSC structure; (b) Energy levels of OSC materials.

Then, the charge carrier generation rate (G) was computed using the following equation.

$$G(x) = PG_{exc}(x) = KH(x) \qquad (14)$$

where

$$K = P\frac{\lambda}{hc}\alpha_j\frac{\eta_j}{\eta_0}\left|t_j^+\right|^2 I_0$$

IV. ENERGY, FIELD, POTENTIAL & CURRENT IN OSC

The structure, energy bands, electric fields, potentials, and currents related to organic solar cells (OSCs) are described in this section. Fig. 2(a) presents the structure of the OSC analyzed in this study. The layer materials were ITO, PEDOT, PSS, P3HT, PCBM, and *Al*. Among them, ITO works to collect holes to function as an anode terminal, the advantage of using ITO is its transparency, which is suitable for optical devices. PEDOT:PSS (a mixture of PEDOT and PSS) helps to guide and collect holes effectively. P3HT:PCBM (mixture of P3HT and PCBM) is the active layer that absorbs photons (light). *Al*-layer was used to collect electrons to work as the cathode terminal. Fig. 2(b) presents the energy of the layer materials of OSC, which were collected from the literature [5], [12], [36]–[40]. The energy levels are negative because the electron energy is shown here.

The properties of organic materials are described using the lowest unoccupied molecular orbital (LUMO), highest occupied molecular orbital (HOMO), and energy gap separating the LUMO and HOMO.

The bandgap of P3HT (1.9 eV) and PCBM (1.8 eV) suggests that both materials are suitable for absorbing solar irradiance; therefore, excitons are generated in both; for an

exciton generated in an organic material (P3HT or PCBM), the electron of that exciton will be at the LUMO, and the hole at the HOMO of that material.

Some of the excitons are lost because of direct recombination as follows: electrons at P3HT_LUMO fall into holes at P3HT_HOMO or electrons at PCBM_LUMO fall into holes at PCBM_HOMO. The other excitons dissociate into free electrons and holes. Like any other particles, electrons move from high energy to low energy; that is, free electrons will move from P3HT_LUMO to PCBM_LUMO, as shown in Fig. 2(b). For this reason, P3HT is termed as the (electron) donor and PCBM as the (electron) acceptor.

Let us now consider hole movement. The typical energy band diagram shows the electron energy (negative value), as shown in Fig. 2(b). Because hole-energy is positively valued, a hole-energy-band-diagram may be obtained by flipping the electron-energy-band-diagram about the horizontal axis at zero energy. In this case, a high level in the electron-energy-band-diagram will become low in the hole-energy-band-diagram and vice versa. Free holes will move from high hole energy ($\equiv$ low electron energy) to low hole energy ($\equiv$ high electron energy). So, free holes will flow from PCBM_HOMO to P3HT_HOMO as in Fig. 2(b).

Now, electrons at PCBM_LUMO and holes at P3HT_HOMO will form "geminate pairs". The electric field across the active layer breaks these geminate pairs, and hence, electrons and holes will finally become free. Then, they move toward the collecting electrodes.

When an electrode is attached to one side of the active layer (mixer of P3HT and PCBM), some regions of the electrode are in touch with P3HT and some regions with PCBM. Electrons at PCBM_LUMO or holes at P3HT_HOMO will choose the electrode to move depending on the energy. If the energy level of the electrode material is slightly (not largely) less than that of PCBM_LUMO, then free electrons will move from PCBM_LUMO to that electrode through a feasible small energy change, here free electrons will move to *Al*, hence *Al* will work as a cathode. On the other hand, if the energy level of the electrode material is slightly higher than that of P3HT_HOMO, then free holes will move from P3HT_HOMO to that electrode, here free holes will move to PEDOT:PSS and then to ITO; hence, ITO will work as an anode. Inside the OSC, both electron-flow and hole-flow will create current flowing from PCBM to P3HT. Outside the OSC, when a load is connected, the current will come out at the ITO (P3HT side), go through the load, and enter at *Al* (PCBM side).

The PEDOT:PSS layer was used for better collection of holes. The movement of holes directly from P3HT_HOMO to ITO would not be effective because it would require a large energy change that is not naturally favorable. The PEDOT:PSS layer between P3HT and ITO creates a gradual small energy difference between two adjacent layers so that holes can move through favorable small energy changes in two steps; thus, holes are guided towards ITO and effectively collected. A similar approach can be used to guide electrons, if necessary.

Let us look at pn junction solar cell. A pn junction has an internal electric field directed from the n-side to the p-side, and a corresponding built-in potential (V_{bi}). When light is incident on a pn junction, holes and electrons are generated, and a current is produced by the field in the direction from n-side to p-side. Usually, the direction from p-side to n-side is considered as positive; therefore, the field and current of a pn junction solar cell are negative.

We already know that the current inside the OSC is from PCBM to P3HT, whereas the current inside the pn junction solar cell is from n-side to p-side. By comparison, it may be deduced that PCBM is like n-side and P3HT is like p-side.

The active layer (mixer of P3HT and PCBM) is similar to a single metamaterial, where PCBM_LUMO is equivalent to the conduction band and P3HT_HOMO is equivalent to the valence band [10], [11], [13], [15]. OSC has a current, hence it has an internal electric field and a corresponding built-in potential (V_{bi}) like pn junction. Literature [13], [15], [36] shows that the energy levels of *Al* and PEDOT:PSS may be considered as the Fermi levels and the difference between them will determine the value of V_{bi}; that is, $V_{bi} = (E_{Al} - E_{PEDOT:PSS})$ volts.

Solar cell current may be used instantly by flowing it through a load connected at solar cell terminals; in this case, the load will receive solar power while the sun is available. Usually, a solar cell current is used to charge a battery to store solar power for later use, especially when the sun is absent. When a battery is charged by an organic solar cell (OSC), the battery terminal connected to ITO becomes positive polarity and the battery terminal connected to *Al* becomes negative polarity because the current comes out at ITO, goes through the battery, and then enters into *Al*. The voltage of the connected battery (being charged) affects the OSC current by working as an external applied voltage (V_a), which gives a positive voltage to ITO (P3HT side, p side) and negative voltage to *Al* (PCBM side, n side). This indicates that V_a produces a positive current in the forward direction, working against V_{bi}. Therefore, the resultant electric field (F) can be approximated as $F = (V_a - V_{bi})/d_j$, where d_j = active layer thickness.

Like many other researchers [11], [13], [14], [15], this work also assumes F to be constant throughout the active layer, which is valid if the active layer thickness (d_j) is low (≤ 200 nm).

While moving, some electrons and holes will be recombined inside the active layer; this recombination was considered in this work.

Here, E_{d0p} and E_{djp} are the energy differences between the valence band (P3HT_HOMO) and Fermi levels at $x = 0$ and $x = d_j$ shown in Fig. 2(b); E_{d0n} and E_{djn} are the energy differences between the conduction band (PCMB_LUMO) and Fermi levels at $x = 0$ and $x = d_j$. These energy differences were used as boundary conditions to solve the differential equations for the holes and electrons.

V. UNIVERSAL SOLUTION FOR HOLE & ELECTRON

Organic solar cells (OSCs) and semiconductor pn junctions are analogous, but their structures are different; therefore, the approaches of analyses are different. The pn junction has a small depletion layer around the junction that contains charged atoms, producing an internal electric field. The field force produces drift current. Again, the concentration difference of holes (or electrons) at the two sides of the depletion layer produces diffusion current. In forward bias, the diffusion current is much larger than the drift current; therefore, the drift current is neglected, and only the diffusion current is considered for calculating the current. On the other hand, in reverse bias, no diffusion current exists, and only the drift current is considered. However, for bulk heterojunction OSCs, the active layer is the mixer of donor and acceptor materials (no distinct separating boundary), and the concentration difference of holes (or electrons) exists throughout the active layer, and the electric field is across the entire active layer (not across the small depletion layer); therefore, diffusion and drift currents exist throughout the entire active layer; hence, both currents are to be considered in the calculation of current in OSCs.

Because of the various interactions inside the device, all the generated electrons and holes cannot participate in the current production. The current-producing hole (electron) density per unit volume can be determined using the drift-diffusion transport equation, continuity equation, charge carrier generation rate, and recombination rate. The analytical expression of the hole (electron) is derived first, followed by the analytical expression of its current.

Let us first consider the case of current-producing holes (p). If an electric field exists in the positive x direction, holes will drift in the positive x direction, producing a drift current ($q\mu_p Fp$) in the positive x direction. If the hole concentration gradient exists and dp/dx is positive, holes will diffuse toward the negative x direction, producing a diffusion current ($k_B T \mu_p dp/dx$) in the negative x direction. Therefore, the transport equation for holes is as follows [41]:

$$J_p = q\mu_p Fp - k_B T \mu_p \frac{dp}{dx} \tag{15}$$

The continuity equation for holes is

$$\frac{1}{q}\frac{dJ_p}{dx} = (G - R_p) \tag{16}$$

where J = current density, G = generation rate, R = recombination rate.

Similarly, in the case of current-producing electrons (n), if an electric field exists in the positive x direction, electrons will drift in the negative x direction, producing a drift current ($q\mu_n Fn$) in the positive x direction. If the electron concentration gradient exists and dn/dx is positive, electrons will diffuse toward the negative x direction, producing a diffusion current ($k_B T \mu_n dn/dx$) in the positive x direction. Therefore, the transport equation for electrons is as follows [41]:

$$J_n = q\mu_n Fn + k_B T \mu_n \frac{dn}{dx} \tag{17}$$

The continuity equation for electrons is

$$-\frac{1}{q}\frac{dJ_n}{dx} = (G - R_n) \tag{18}$$

From the above four equations, it can be seen that if we consider the values of q and μ with negative sign in Eqs. (15) and (16) then they become the same as in Eqs. (17) and (18), therefore, we can use two equations instead of four. That is, in general, for any charge carrier (Q), we may use the following two Eqs. (19) and (20), we can obtain a universal solution for both holes and electrons. To obtain the results for holes, we have to use the values of q and μ with positive sign; on the other hand, to obtain the results for electrons, we have to use the values of q and μ with negative sign.

$$J = q\mu FQ - k_B T \mu \frac{dQ}{dx} \tag{19}$$

$$\frac{1}{q}\frac{dJ}{dx} = (G - R_Q) \tag{20}$$

where Q = hole (electron) density (unit: m^{-3}), J = hole (electron) current density (unit: Am^{-2}), G = hole (electron) generation rate (unit: s^{-1}m^{-3}), R_Q = recombination rate = $r_m Q$; r_m = monomolecular recombination coefficient (s^{-1}).

Using Eqs. (19) and (20), we get

$$\frac{d^2Q}{dx^2} + a_1 \frac{dQ}{dx} + a_2 Q = a_3 G \tag{21}$$

a_1, a_2, and a_3 are defined in Appendix C.

When there is no light (dark condition), charge carriers are generated because of the environmental temperature. When light is incident, environmental temperature is also present; therefore, we have to calculate the charge carriers generated by the incident light (photo component) as well as by the environmental temperature (dark component).

For charge carriers produced by dark condition the differential equation is

$$\frac{d^2Q}{dx^2} + a_1 \frac{dQ}{dx} + a_2 Q = 0 \, [\because G = 0] \tag{22}$$

The solution of Eq. (22) is

$$Q_{dark} = A_1 e^{\omega_1 x} + A_2 e^{\omega_2 x} \tag{23}$$

ω_1 and ω_2 are defined in Appendix C. Again, A_1 and A_2 are constants to be determined using boundary conditions.

For charge carriers produced by photons, the differential equation is

$$\frac{d^2Q}{dx^2} + a_1 \frac{dQ}{dx} + a_2 Q = a_3 G \, [\because G \neq 0] \tag{24}$$

Complementary solution of Eq. (24) is

$$Q_{ph1} = A_3 e^{\omega_1 x} + A_4 e^{\omega_2 x} \tag{25}$$

Here A_3 and A_4 are constants to be determined using boundary conditions.

Using G from Eq. (14), which is for a single wavelength, we can get a particular solution of Eq. (24) as follows [31]:

$$Q_{ph2} = a_4 e^{-\alpha_j x} + a_5 e^{\alpha_j x} + a_6 cos\,(N - Rx)$$
$$+ a_7 sin\,(N - Rx) \quad (26)$$

a_4, a_5, a_6, and a_7 are defined in Appendix C.

Total solution of Eq. (24) is

$$Q_{ph} = A_3 e^{\omega_1 x} + A_4 e^{\omega_2 x} + a_4 e^{-\alpha_j x} + a_5 e^{\alpha_j x}$$
$$+ a_6 cos\,(N - Rx) + a_7 sin\,(N - Rx) \quad (27)$$

Eq. (27) represents the photo-charge carriers for a single wavelength.

Photo-charge carriers for all wavelengths can be found as

$$Q_{pht} = \int_{\lambda_1}^{\lambda_2} Q_{ph} d\lambda \quad (28)$$

Total charge carriers (dark plus photo) may be calculated as follows:

$$Q = Q_{dark} + \int_{\lambda_1}^{\lambda_2} Q_{ph} d\lambda \quad (29)$$

Eq. (29) is the universal expression for evaluating both holes (h) and electrons (n). That is, $h = Q$ (calculated with positive μ, q) and $n = Q$ (calculated with negative μ, q).

The boundary values of the charge carriers at $x = 0$ and $x = d_j$ were calculated using the energy levels in the standard equations of semiconductor physics [41], and then applying these boundary values in Eq. (29), we can calculate A_1, A_2, A_3, and A_4. The detailed calculations are given in Appendix D.

Let us now consider current calculations. By substituting Q_{dark} from Eq. (23) into Eq. (19), we can obtain the dark current as

$$J_{Qdark} = A_{11} e^{\omega_1 x} + A_{12} e^{\omega_2 x} \quad (30)$$

A_{11} and A_{12} are defined in Appendix E.

Again, by substituting Q_{ph} from Eq. (27) into Eq. (19), we can obtain the photocurrent for a single wavelength as

$$J_{Qph} = A_{21} e^{\omega_1 x} + A_{22} e^{\omega_2 x} + A_{23} e^{-\alpha_j x} + A_{24} e^{\alpha_j x}$$
$$+ A_{25} cos\,(N - Rx) + A_{26} sin\,(N - Rx) \quad (31)$$

$A_{21}, A_{22}, A_{23}, A_{24}, A_{25}$, and A_{26} are defined in Appendix E.

Photocurrent for all wavelengths is

$$J_{Qpht} = \int_{\lambda_1}^{\lambda_2} J_{Qph} d\lambda \quad (32)$$

Total current (dark plus photo) of any charge carrier is

$$J_Q = J_{Qdark} + \int_{\lambda_1}^{\lambda_2} J_{Qph} d\lambda \quad (33)$$

Eq. (33) is the universal equation for evaluating both the hole current (J_p) and electron current (J_n). That is, $J_p = J_Q$ (calculated with positive μ, q) and $J_n = J_Q$ (calculated with negative μ, q).

Grand total current due to both holes and electrons is

$$J_{total} = J_p + J_n \quad (34)$$

VI. RESULTS AND DISCUSSIONS

Solar cell analysis using an analytical method requires information on the sunlight intensity (irradiance), whose surface value is 6.33×10^7 W/m^2, and it is decreased to 1367 W/m^2 while the light reaches just outside the atmosphere above the earth, which is known as extraterrestrial irradiance. The light intensity is further reduced because of absorption by the atmosphere. The amount of absorption depends on whether the light travels through the Earth's atmosphere in the perpendicular direction (shortest distance) or in the inclined direction (longer distance) to reach a place on the earth where the solar cell is situated. The condition of inclination is indexed by the air mass (AM), which is the ratio of the actual traveled distance through the atmosphere to the perpendicular distance. Extraterrestrial irradiance is indexed by AM 0 because light travels no distance through the atmosphere. When the light reaches a place on the earth in the perpendicular direction, it is indexed by AM 1.0. When the light comes at an angle of 60^0, it crosses the distance double the perpendicular distance; it is indexed by AM 2.0. Solar irradiance of AM 1.5 (global) was used in this work, as in many other studies [2], [3], [9], [12], [15], [22]. The data of irradiance AM 1.5 were collected from standard sources [42].

To calculate the excitons using the optical transfer matrix method, we need the refractive index (η) and extinction coefficient (κ) of the materials of the device under investigation, which were collected from the literature [26], [36].

To obtain the photo-excited part of any quantity, it is necessary to integrate over the effective wavelength range. The effective wavelength range depends on the device structure and the layer materials. It is essential to identify the precise effective wavelength range for two reasons: (i) to understand which portion of the solar spectra would be absorbed by a device structure, it would be useful to compare the optical effectiveness of different structures and determine the best one; (ii) experimental works are usually performed with different levels of input power (1000 W/m^2, 800 W/m^2, etc.), whereas analytical calculations are usually carried out using solar irradiance AM 1.5, where solar irradiance is expressed in units of Wm^{-2}nm^{-1}. To compare the experimental and analytical results, the input power for both cases should be the same. To determine the input power level in the analytical calculation, we need to integrate the solar irradiance over the exact effective wavelength range that a device actually absorbs; if the calculated (integrated) power is not the same as the experimental input power level, then the input solar irradiance is multiplied by a factor before using it in the analytical calculation to ensure that the input power level of the analytical calculation is equal to the input power level of the experiment. The multiplying factor is the ratio of the experimental input power to the power obtained by

integrating the solar irradiance over the exact effective wavelength range.

Excitons represent the absorption amount; therefore, excitons were investigated to obtain the exact effective wavelength range of the OSC structure in Fig. 2(a). First, the lower limit of wavelength was fixed at 350 nm, and the upper limit was varied in the range of 350 to 850 nm. For a selected upper limit value, the exciton generation rate at a certain position was calculated for each wavelength using Eq. (9), the results were integrated over the wavelength range extending from the lower limit (350 nm) to the upper limit (selected value). Similarly, integrated values were calculated for the other positions. Then, the average exciton was calculated by averaging the integrated values of all the positions. Similarly, the average excitons were determined for the other selected upper limit values. Fig. 3(a) shows the average excitons computed with solar irradiance of AM 1.5; the exciton increases with the upper limit; for a fixed lower limit, increasing the upper limit encompasses more wavelengths (photons); hence, the exciton increases. For the upper limit of 730 nm or more, the average exciton generation rate reaches 4.9×10^{27} $s^{-1}m^{-3}$ (for irradiance AM 1.5) and does not increase further, as shown in Fig. 3(a), indicating that photons with wavelengths greater than 730 nm do not contribute, that means the device does not absorb; therefore, the exact upper limit is 730 nm. Similarly, another calculation was carried out, keeping the upper limit fixed at 850 nm and varying the lower limit in the range of 850 to 350 nm. For each selected lower limit value, the average exciton was calculated as described above and is plotted in Fig. 3(b). In this case, the average exciton increases with the decrease of the lower limit; for a fixed upper limit, the decreasing lower limit encompasses more wavelengths (photons); hence, the exciton increases. For the lower limit of 360 nm or less, the average exciton no longer increases, indicating that the exact lower limit is 360 nm.

To verify the applicability of the optical transfer matrix method, the optical electric field magnitudes at different positions inside the active layer of the OSC were calculated using the OTMM-based Eq. (7). Note that Eq. (7) determines the square of the field magnitude, however, the field magnitudes have been presented here. Fig. 4 presents the positional variation of the optical electric field magnitudes for an OSC with the active layer thickness (d_j) of 100, 200, and 300 nm for different irradiances (400 to 1000 W/m^2).

As expected, the optical electric field was found to be larger for higher irradiances. The optical electric field variation exhibits a wave-like pattern with positions as shown in figure, not constant, and not exponential, indicating that OTMM includes the optical phenomena (reflection, refraction, interference) and hence provides the correct distribution (profile) of light. Because the optical electric field produces excitons and charge carriers, they also exhibit similar wave-like variations with positions. Optical field varies in the range of 0.1 to 0.6 V/m as shown in Fig. 4. For the device with active layer thickness of 100 nm, the excitons are found
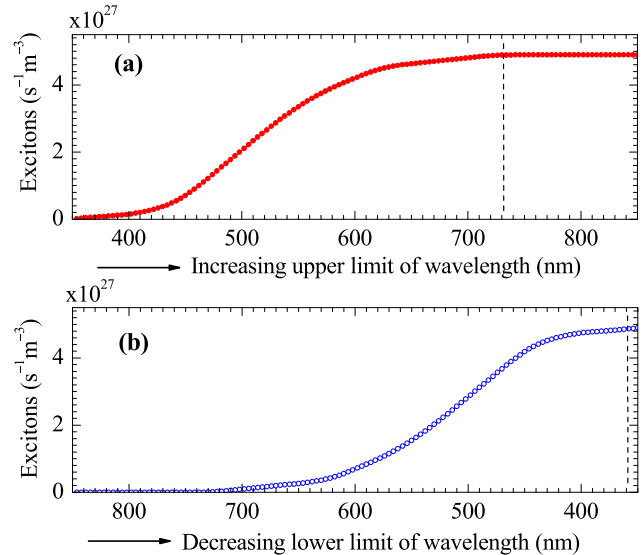

FIGURE 3. Average excitation generation rate of OSC with irradiance of AM 1.5 (global), active layer thickness of 100 nm: (a) when lower limit of wavelength is fixed at 350 nm and upper limit is increasing, (b) when upper limit is fixed at 850 nm and lower limit is decreasing.

varying in the range of 1×10^{27} to $16 \times 10^{27} s^{-1}m^{-3}$ with the average excitons of 4.3×10^{27}, 6.4×10^{27}, 8.5×10^{27}, and 10.6×10^{27} $s^{-1}m^{-3}$ for irradiances of 400, 600, 800, and 1000 W/m^2, respectively, these values are consistent with other works [10], [17], [43].

Regarding the dissociation probability of excitons, previous work [31] showed that Braun's formulation estimates high probability; Wojcik's formulation estimates low probability; however, the probability calculated by incorporating the spherically averaged Gaussian distribution (SAGD) function gives the value between the two. Naturally, the separation distances of electrons and holes of excitons are different; because of considering this natural fact in the SAGD-incorporated dissociation probability, it has been assumed to be logical. Using the SAGD-incorporated probability, the charge carriers were calculated using Eq. (14).

The current-producing hole density (unit: m^{-3}) was calculated analytically using Eq. (29) with positive q and μ; similarly, the electron density was determined using Eq. (29) with negative q and μ; this universal Eq. (29) was obtained from the analytical solution of the differential Eq. (21). Now, the same differential Eq. (21) was solved using a numerical method and plotted along with the analytical results.

Fig. 5 shows the analytical and numerical results for the hole and electron densities with positions for an irradiance of 1000 W/m^2 and terminal voltages (V_a) of 0.1, 0.3, and 0.5 V. Analytical results (solid line) exactly match the numerical results (markers) for each case as shown, which ensures the correctness of the analytical solution.

Another universal analytical Eq. (33) was derived and used to calculate the hole and electron currents. The total current was obtained using Eq. (34). The total current, calculated
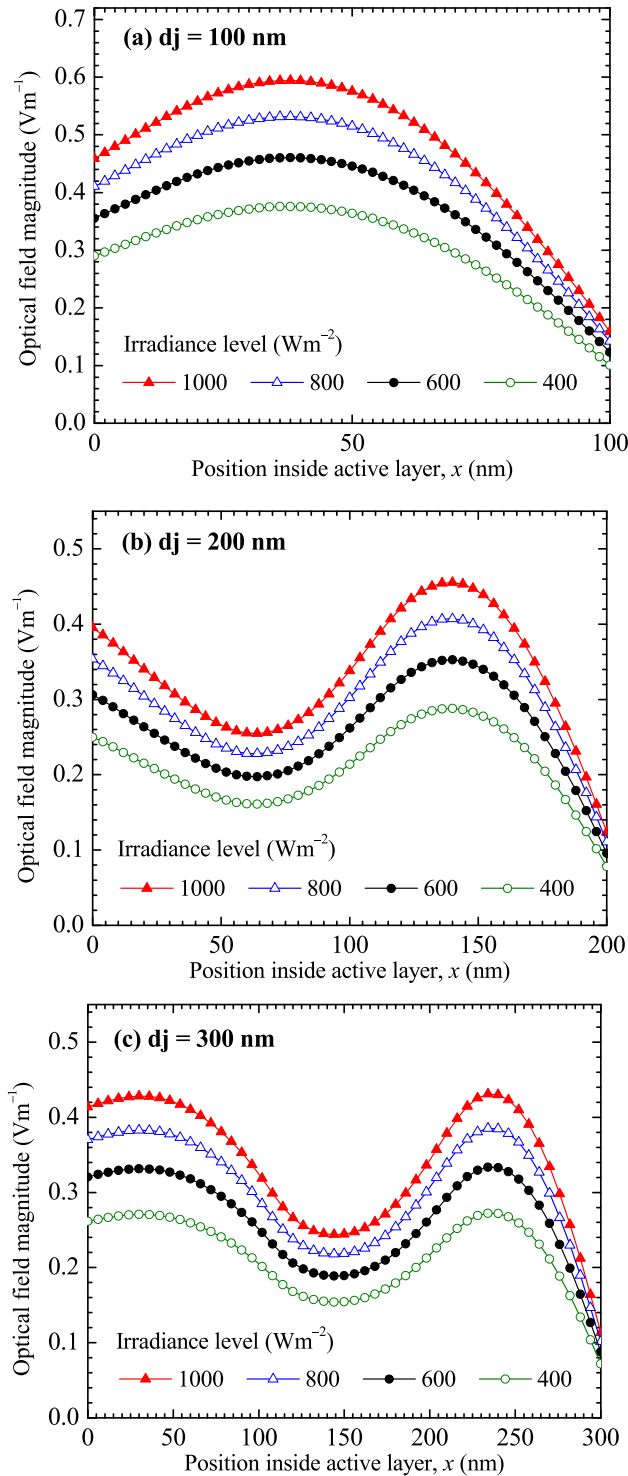
FIGURE 4. Optical electric field magnitude of an organic solar cell for irradiance of 400 to 1000 W/m² having the active layer thickness of (a) 100 nm, (b) 200 nm, and (c) 300 nm. Optical electric field magnitudes are different at different positions due to optical reflection, refraction and interference.

using the constant value of the recombination coefficient, was found to vary with the positions, as shown in Fig. 6, which is inconsistent because the total current should be the same at all positions.
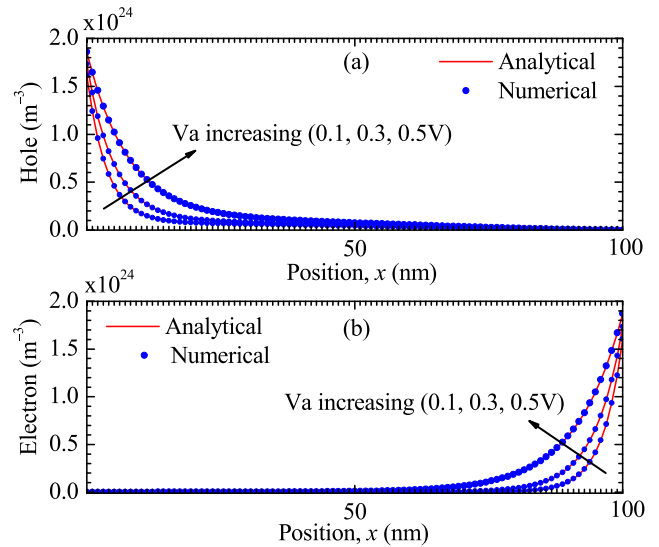

FIGURE 5. Current-producing hole and electron density with positions inside active layer of OSC for irradiance 1000 W/m². Analytical (solid line) and numerical (markers) results are found exactly matched with each other.
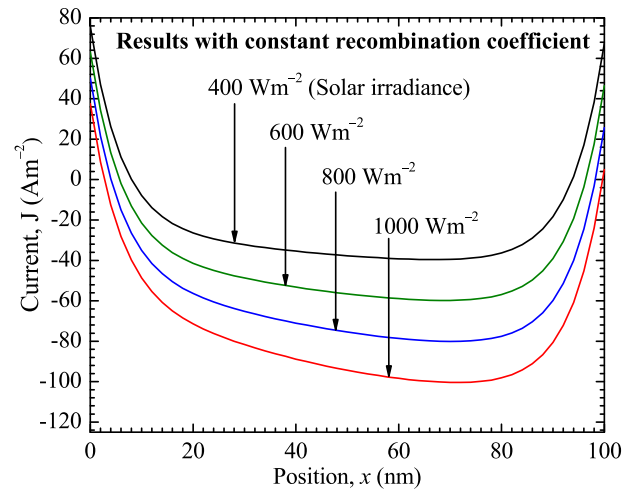

FIGURE 6. Total current calculated using constant recombination coefficient, terminal voltage of 0.4 V and irradiance power levels of 400, 600, 800, 1000 W/m². Total current values are found different at different positions, which is inconsistent with position-independent property of total current.

Other researchers [26]–[29], who used a constant recombination coefficient, also observed the position dependency of the total current; however, they presented the value of current at a certain position or the average value of current in their reports. Again, those [30] who neglected recombination in the analytical solution found the current to be the same at all positions. However, recombination cannot be neglected, especially for devices that are highly recombination prone. To obtain a consistent position-independent current, we must use the appropriate positional values of the recombination coefficient instead of using a constant value. This is logical because, owing to optical interference and differences in mobility, the hole and electron densities would be
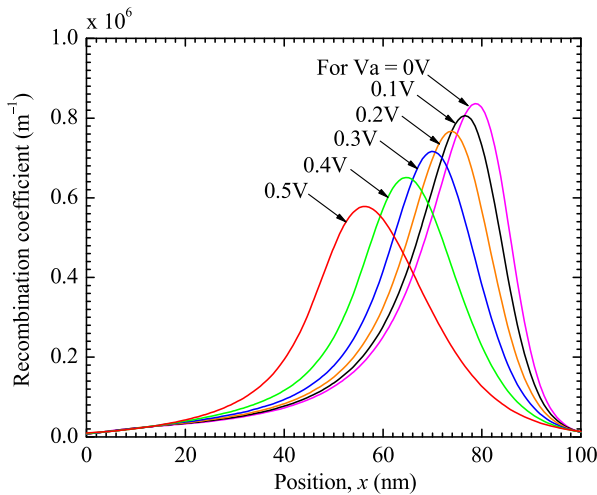
FIGURE 7. Extracted recombination coefficients with positions inside active layer of an OSC with irradiance 1000 W/m², terminal voltage (V_a) values of 0 to 0.5 V. With the increase of V_a, the peak value of spatial recombination coefficient decreases, and peak position shifts leftwards.
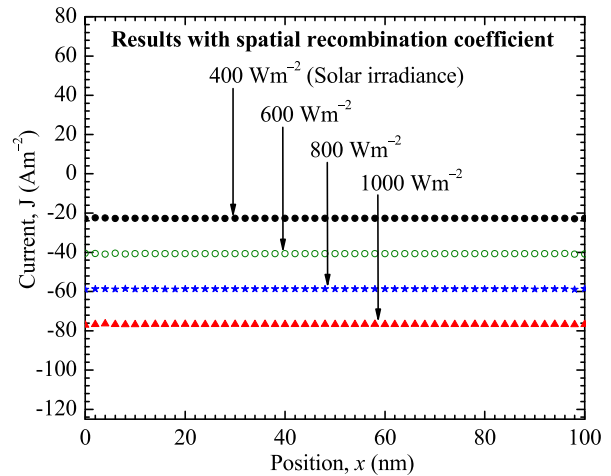

FIGURE 8. Total current calculated using spatial recombination coefficients, terminal voltage of 0.4 V and irradiance levels of 400, 600, 800 and 1000 W/m². Total current values are found same at all positions, which is consistent with position-independent property of total current.

different at different positions; hence, recombination would be different.

The positional values of the recombination coefficients were extracted using the following procedure. For a certain irradiance power and a certain terminal voltage, the total current at a certain position was calculated analytically using Eq. (34) by varying the recombination coefficient over a wide range, the value of the recombination coefficient, for which the calculated current matches with the experimental value, is accepted as the appropriate recombination coefficient for that position. Similarly, the recombination coefficients for the other positions were extracted. Similarly, for the other terminal voltages, the positional values of the recombination coefficients were extracted. Similar calculations were performed for other irradiance levels. As expected, the extracted values of the recombination coefficients were found to be different at different positions.

Fig. 7 exhibits spatial variation of extracted recombination coefficients inside active layer of an OSC for irradiance 1000 W/m², terminal voltage (V_a) of 0, 0.1, 0.2, 0.3, 0.4, and 0.5V; peak values and peak positions are different for different terminal voltages. It has already been mentioned that the resultant electric field $F = (V_a - V_{bi})/d_j$. Because V_a cannot be larger than V_{bi} and V_{bi} is fixed, with the increase of V_a (increase of battery charging), the field F remains negative, but the magnitude of the field decreases. For lower V_a, the field magnitude is higher; hence, more excitons are dissociated, more charge carriers are generated, and more recombination occurs because recombination is directly proportional to the population of charge carriers; therefore, the peak level of the recombination coefficient is higher for lower V_a. In contrast, if V_a is increased, the peak level of the recombination coefficient decreases, as shown in Fig. 7.

We know that the field is negative, directed in the negative x, right to left in Fig. 2(b). For a lower V_a, the field

magnitude is higher; for higher fields, most of the charge carriers are generated closer to the right edge of the active layer (closer to the surface of the start of field), which is similar to the skin effect (tendency to crowd near the surface); therefore, higher recombination occurs closer to the right edge, that is, the peak of the recombination coefficient occurs closer to the right edge for a lower V_a. Accordingly, if V_a is increased, the peak position shifts leftward, as shown in Fig. 7. The values of the recombination coefficient were found to vary in the order of $10^4 - 10^6$ m^{-1}.

Then, using these extracted spatial recombination coefficients, the total current was calculated by the Eq. (34). The total current was found to have the same value at all positions, as shown in Fig. 8, which is consistent with the position-independent property of the total current.

Note that, using the spatial recombination coefficient, Eq. (34) gives the total current directly and does not need to have an average. Thus, by using the spatial recombination coefficient, the problem of the position dependency of the total current can be solved.

To gain further insight, the hole and electron currents were calculated separately using Eq. (33) with positive q, μ and negative q, μ, respectively. Fig. 9 shows the variation of the hole current, electron current, and total current with position (x) for an OSC with a terminal voltage of 0V, an active layer thickness of 100 nm, and an irradiance of 1000 W/m². Here, both the hole current and electron current are negative; therefore, the total current is negative. The hole current magnitude decreases with position, whereas the electron current magnitude increases, as shown in Fig. 9; hence, their summation, that is, the total current magnitude is constant with position.

The electric field produces drift current. Because the field is negative, the drift currents of holes and electrons are both in the negative x direction. The drift current magnitude is proportional to the magnitude of the electric field and the number
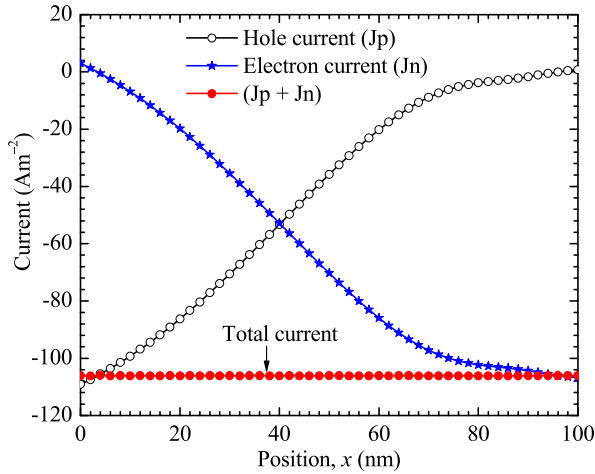
FIGURE 9. Hole current, electron current and total current variation with position. Hole current magnitude decreases, whereas electron current magnitude increases, therefore, the summation of them gives the same value at each position, that is, total current is constant for all positions.

Current, J (Am⁻²) vs. Terminal voltage, Va (V)

FIGURE 10. Dark current, photo current and total current of OSC for V_a = 0 to 0.6 V (solar cell operation range) with four irradiance levels: (a) 1000 W/m², (b) 800 W/m², (c) 600 W/m², (d) 400 W/m². Analytical total current (solid line) are found consistent with that of experimental measurement (circular markers) for each case.

of charge carriers. For a certain terminal voltage, the electric field magnitude is assumed to be constant throughout the active layer, hence the drift current directly varies with the amount of charge carriers. Fig. 5 shows that the hole (electron) amount is the highest (lowest) at $x = 0$ and decreases (increases) with position; therefore, the hole (electron) negative drift current magnitude is the highest (lowest) at $x = 0$ and decreases (increases) with position.

Again, the concentration gradient (slope) produces diffusion current. As per the concentration profile in Fig. 5, holes (electrons) diffuse in the positive (negative) x direction; hence, the diffusion currents of holes and electrons are both in the positive x direction. The diffusion current magnitude is proportional to the magnitude of the concentration gradient (slope). Fig. 5 shows that the gradient (slope) of the hole (electron) concentration is the highest (lowest) at $x = 0$ and decreases (increases) with position; therefore, the hole (electron) positive diffusion current magnitude is the highest (lowest) at $x = 0$ and decreases (increases) with position. We can summarize as, with position x, the hole (electron) negative drift current magnitude decreases (increases), and the hole (electron) positive diffusion current magnitude decreases (increases).

Fig. 9 shows that both hole and electron currents are negative, this indicates that the hole (electron) negative drift current magnitude is larger than the hole (electron) positive diffusion current magnitude, this also indicates that the decrease (increase) rate of the hole (electron) negative drift current magnitude is larger than the decrease (increase) rate of the hole (electron) positive diffusion current magnitude.

To investigate the current components, the dark current, photocurrent, and total current were calculated analytically using Eqs. (30), (32), and (34), respectively, using the spatial recombination coefficients. Fig. 10 shows the total current and its components with the variation of terminal voltage
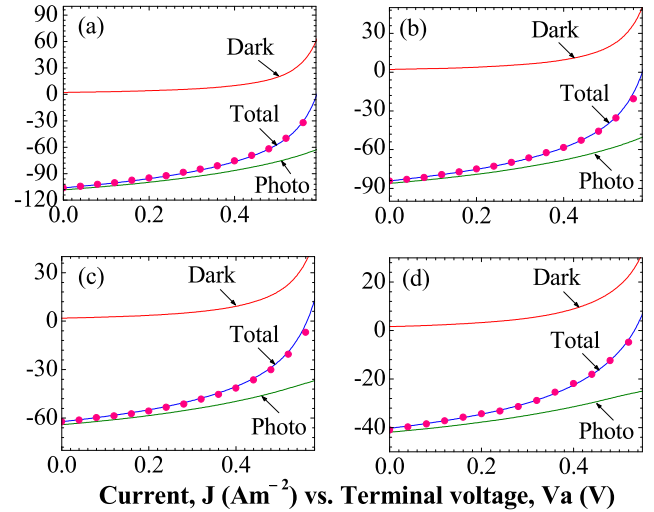
(V_a) for irradiances of 1000, 800, 600, and 400 W/m². In solar cells, charge carriers are generated by environmental temperature (dark condition) and by photons (illuminated condition). The negative field causes these charge carriers to flow and produces a current in the negative direction (reverse current). On the other hand, the charging battery voltage (V_a) is connected at the terminal in such a way that it produces current in the positive direction (forward current).

Under dark condition, there are thermally generated charge carriers; they are few in number, and the reverse current due to these few thermal charge carriers is negligible and hence solved with zero generation rate, but there is V_a applied at the terminal; therefore, the dark current is a positive forward current due to V_a, which is similar to the forward bias current of a pn junction, as shown in Fig. 10.

Under illuminated condition, there are photo-generated charge carriers, which are large in number, and the reverse current due to these large photo charge carriers is not negligible and hence solved including generation rate, in addition there is V_a applied at the terminal; therefore, the photocurrent is determined by the generation rate and V_a. In this case, V_a modifies the resultant electric field and hence affects the photocurrent. The resultant electric field $F = (V_a - V_{bi})/d_j$. At the start of battery charging, $V_a = 0$, hence the resultant field $F = -V_{bi}/d_j$ is negative, so the photocurrent is negative, and this field magnitude is the maximum; as a result, the highest excitons are dissociated; hence, this negative photocurrent magnitude is the maximum. As V_a increases, the field magnitude decreases; as a result, fewer excitons are dissociated; hence, the negative photocurrent magnitude decreases, as shown in Fig. 10.

That is, with the increase of V_a, there are two effects: (i) the positive dark current magnitude increases from zero,

TABLE 1. Parameter values used in this work.

Parameter	For hole	For electron
Planck's constant (h)	6.626×10^{-34} Js	
Light speed (c)	3×10^8 m/s	
Relative permittivity (ϵ_r)	3.5	
Air permittivity (ϵ_0)	8.854×10^{-12} F/m	
Boltzmann's constant (k_B)	1.38×10^{-23} J/K	
Internal voltage (V_{bi})	0.8 V	
Temperature (T)	300 K	
Reactivity parameter (S_r)	0.05 cm/s	
Separation distance (r)	Variable	
Sep. for Gaussian peak (r_a)	1.65 nm	
Recombination coef. (r_m)	Extracted spatial values	
Density of states (N_s)	10^{26} m^{-3}	
Thermal energy (E_t) [$= k_B T$]	0.0259 eV (4.14×10^{-21} J)	
Mobility (μ) [m^2 V^{-1} s^{-1}]	0.1×10^{-8}	-7×10^{-8}
Electronic charge (q)	1.6×10^{-19} C	-1.6×10^{-19} C
Energy diff. at $x = 0$ (E_{d0})	0.1 eV	0.9 eV
Energy diff. at $x = d_j$ (E_{dj})	0.9 eV	0.1 eV

FIGURE 11. Variation of current with solar irradiance. Current increases linearly with irradiance. For a certain irradiance, lower current at higher terminal voltage and vice vera. Analytical results (solid line) match with experimental ones (markers).

and (ii) the negative photocurrent magnitude decreases from the maximum negative value. As a result, the total current (dark plus photo) is maximum negative at first, then the negative total current magnitude decreases and approaches toward positive value. When the increased positive dark current magnitude becomes equal to the decreased negative photocurrent magnitude, the total current becomes zero, the battery charging stops, solar cell operation ends, V_a value at this point is the open circuit voltage (V_{OC}), whose values were found to be 0.537V, 0.569V, 0.588V, and 0.6V for operation with irradiances of 400, 600, 800, and 1000 W/m^2, respectively. Note that, for the OSC structure in Fig. 2, $V_{bi} = (E_{Al} - E_{PEDOT:PSS}) = -4.3 - (-5.1) = 0.8V$. Each value of V_{OC} obtained is less than V_{bi} (= 0.8V). The analytical result of the total current (solid line) is found to match with the experimental result (markers) [23] for each irradiance, as shown in Fig. 10. Therefore, it may be assumed that this analytical calculation can accurately predict OSC current (performance).

For solar cell operation, practically, V_a cannot be larger than V_{OC}; however, in the mathematical analysis, if the calculation is continued with V_a value larger than V_{OC}, we will obtain a total current positive, but this current would not be for solar cells; it would be the forward current remaining after compensating for the negative photocurrent. When the device operates as a solar cell, its current is negative, but the terminal voltage (V_a) is positive ($0 \leq V_a \leq V_{OC}$); hence, the power is negative, which indicates that the solar cell delivers power (not consuming power).

The parameter values utilized in this work are listed in Table 1. While fitting the analytical results with experimental values for different irradiances, only the power has been changed, keeping all other parameter values fixed; that is, they are valid for different irradiance levels, and these values are consistent with those used by others [20], [21],
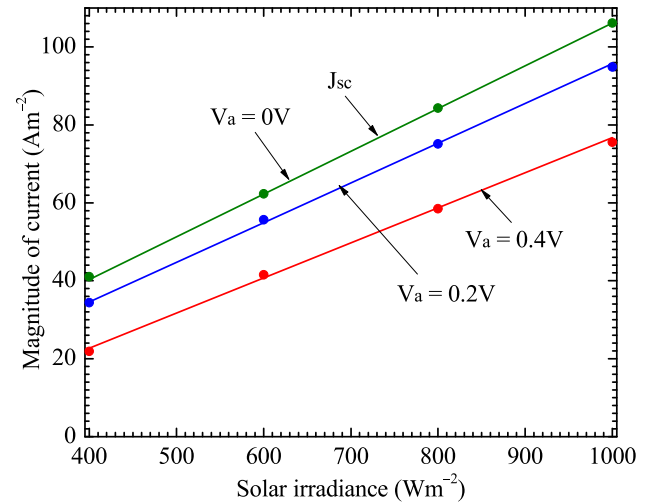
[35], [36], [44], [45]; therefore, these parameter values may be considered acceptable.

Again, the current was investigated with respect to solar irradiance for three terminal voltages (V_a) of 0V, 0.2V, and 0.4V and is plotted in Fig. 11. The current magnitude was found to increase linearly with solar irradiance, as shown in Fig. 11, which is logical because higher irradiance produces more excitons, more charge carriers, and hence more current.

On the other hand, for a certain irradiance level, for a higher V_a less current is obtained, as shown in Fig. 11; for a higher V_a the field magnitude is reduced, fewer excitons are dissociated, and hence less current. The analytical results (solid line) are consistent with the experimental ones (markers) [23].

The current of the OSC was investigated by varying the active layer thickness (d_j). Fig. 12 presents the variation of the OSC current magnitude with the variation of d_j for irradiance of 1000 W/m^2 and terminal voltage (V_a) of 0V, 0.2V and 0.4V. At first, the current magnitude increases with d_j and reaches the highest peak at d_j of around 80 nm, and then shows a pulsating variation with d_j. For some d_j, the meeting of incident and reflected lights in-phase is rigorous, so a peak occurs; for some other d_j, meeting out-of-phase is rigorous, so a dip occurs, resulting in a pulsating pattern, which is consistent with previous reports on photons absorbed, short-circuit current, and efficiency with the variation of d_j [15], [36], [37], [46]. For $d_j = 100$ nm, the experimental result (marker) is found to match with that of analytical computation (solid line) for each case of V_a as shown; hence, it is expected to match for other d_j.

The OSC current depends on the wavelength and hence exhibits spectral variation. The photocurrent of the OSC owing to a single wavelength was calculated using Eq. (31); similarly, photocurrents were calculated for all wavelengths, and thus spectral analysis was performed. Fig. 13 is showing
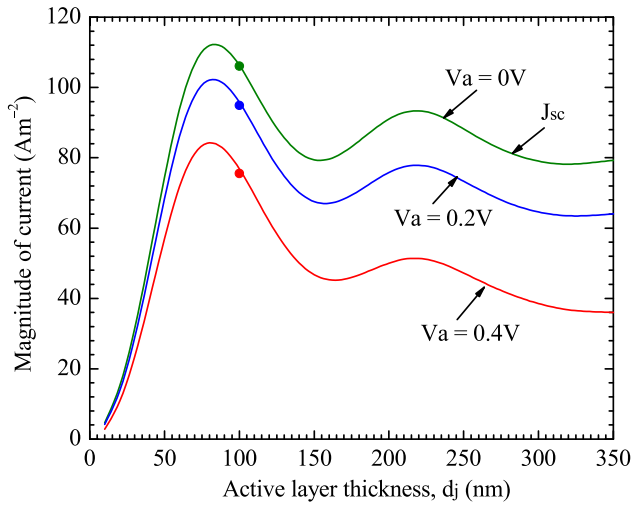
FIGURE 12. Magnitude of OSC current versus active layer thickness (d_j). Current magnitude increases, reaches the highest peak, then exhibits pulsating variation with d_j. For $d_j = 100$ nm, the experimental result (marker) matches with analytical calculation (solid line).

FIGURE 13. Spectral variation of photocurrent of OSC with $d_j = 100$ nm, irradiance = 1000 W/m², terminal voltage V_a = 0V and 0.6V.

the spectral variation of photocurrent of OSC with $d_j = 100$ nm, irradiance = 1000 W/m² and $V_a = 0$V and 0.6V. This shows that photocurrent is available for the wavelength range 360 to 730 nm, which is consistent with previously obtained effective wavelength range. Among them, photons in the wavelength range of $400-650$ nm provide major contributions to the photocurrent; other wavelengths have a negligible effect. For a higher V_a, the photocurrent decreases and vice versa, as shown in Fig. 13. At higher V_a, the electric field magnitude is smaller, so fewer excitons are dissociated, resulting in less photocurrent.

The coefficient constants $A_{21}, A_{22}, A_{23}, A_{24}, A_{25}, A_{26}$ in Eq. (31) depend on $A_3, A_4, a_4, a_5, a_6, a_7$ (see Appendix E). On the other hand, A_3, A_4 depend on a_8, a_9 (see Appendix D). Again, a_8, a_9 depend on a_4, a_5, a_6, a_7 (see Appendix D). Each of a_4, a_5, a_6, a_7 depends on K (see Appendix C). Again, K contains I_0 (see Eq. (14)). That is, the coefficient constants in Eq. (31) depend directly on I_0 (the incident irradiance). In the standard data source, the irradiance I_0 is recorded in unit of $Wm^{-2} nm^{-1}$, that is, W/m² per nm bandwidth of wavelength. Therefore, in Fig. 13, the unit of the photocurrent is $Am^{-2} nm^{-1}$. The photocurrent magnitude was found to vary in the range of 1×10^8 to 7×10^8 $Am^{-2}nm^{-1}$, for an irradiance of 1000 W/m², as shown in Fig. 13. If the photocurrent ($Am^{-2} nm^{-1}$) in Fig. 13 is integrated with respect to wavelength (nm) over the wavelength range, then the photocurrent will be obtained with the unit of Am^{-2}. For the spectra in Fig. 13, the integrated photocurrent magnitudes were found as 108.4 Am^{-2} and 61.4 Am^{-2} for V_a of 0V and 0.6V, respectively, these are consistent with the result in Fig. 10(a) for the irradiance of 1000 W/m². The spectral variation of the photocurrent is consistent with that reported in other studies [47]–[50].

Usually, for a solar cell, the terminal voltage V_a is positive ($0 \leq V_a \leq V_{OC}$). Until now, the device has been analyzed
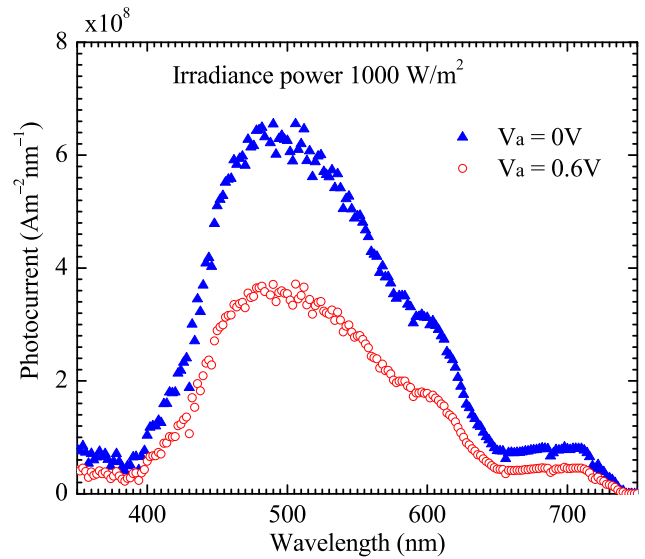
with the positive V_a to determine its performance as a solar cell. However, if a negative V_a is applied, that is, if an already charged battery is connected at the terminal of the device in Fig. 2 with battery-negative at ITO and battery-positive at Al, like the reverse bias of a pn junction, this negative V_a will produce a negative field; hence, the same-directed internal field will be enhanced, which will enhance the dissociation of excitons, and hence a larger negative current is produced. A larger current is easily measurable and detectable; therefore, it is suitable for light sensing; it is a photodiode operation. Therefore, when the device operates with negative V_a, it will not charge the battery, it will not deliver power; instead, an external voltage (battery) is needed; that is, the device will not work as a solar cell; rather, it will work as a light sensor (photodiode). Fig. 14 shows the performance of the device as a photodiode with negative V_a. The current magnitude increases with the increase of negative V_a magnitude because the field is enhanced further, more excitons are dissociated, and hence more current. For a very large negative V_a, there is no significant increase of the current magnitude (almost flat), as shown in Fig. 14, because, the very high field has the ability to dissociate a very large number of excitons, but the number of excitons is limited by the irradiance level.

Both the solar cell and photodiode have the same device structure and working principle, both of which convert light energy to electrical energy. A solar cell is designed (size and material) to have a large amount of absorption (without regard to speed) to work as a good power source, whereas the photodiode is designed to have high speed (without regard to power) to work as a good light sensor. The solar cell is operated in forward bias mode with positive V_a supplied by the battery being charged by the same solar cell; the photodiode is operated in reverse bias mode with negative V_a supplied by the battery already charged; however, for both cases,
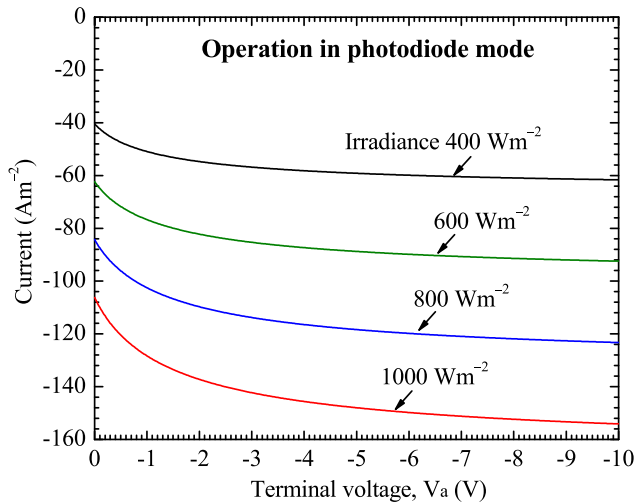
FIGURE 14. The current of P3HT:PCBM based device operated as photodiode with negative terminal voltage (V_a) with irradiance 400, 600, 800, 1000 Wm^{-2}.

the current is negative. That is, the solar cell is operated in the fourth quadrant ($+V$, $-I$) and the photodiode is operated in the third quadrant ($-V$, $-I$) of the current-voltage characteristic graph. In this work, analytical calculations were carried out with positive and negative V_a to investigate the performance of the device for solar cell and photodiode operation.

VII. CONCLUSION

The current of organic solar cells (OSCs) was studied analytically. The investigation of excitons found that the wavelength range of 360 to 730 nm is effective for the investigated device structure. The optical electric field inside the active layer varies from 0.1 to 0.6 V/m. The corresponding exciton generation rate varies in the range of 1×10^{27} to $16 \times 10^{27} s^{-1} m^{-3}$, with average excitons in the range of 4.3×10^{27} to 10.6×10^{27} $s^{-1} m^{-3}$ for irradiance of 400 to 1000 W/m². The charge carriers were calculated from the excitons using an improved dissociation probability, incorporating a Gaussian distribution function. A universal set of solutions was used for both the holes and electrons. The holes (electrons) exhibit exponential variation with position having the highest value of approximately 2×10^{24} m^{-3}. The total current, calculated using a constant recombination coefficient, was found to be position dependent, which is inconsistent. Then, spatial recombination coefficients were extracted, which were found to vary in the order of 10^4 to 10^6 m^{-1}. The total current, calculated using spatial recombination coefficients, was found to be position independent, which is consistent; thus, the problem regarding the position dependency of the total current was solved. The spatial study shows that the hole current magnitude decreases with position, whereas the electron current magnitude increases; hence, their summation (total current) gives a constant value at each position. Again, as the terminal voltage increases, the positive dark current magnitude increases, and the negative photocurrent magnitude decreases; hence, the negative

total current magnitude decreases and becomes zero at the open circuit voltage (V_{OC}). The values of V_{OC} were found to change in the range of 0.5 to 0.6 V for the irradiance of 400 to 1000 W/m². The OSC current varied from 20 to 110 A/m² for irradiances of 400−1000 W/m². Again, the analysis with the active layer thickness (d_j) shows that the OSC current reaches the top at around $d_j = 80$ nm, and then exhibits pulsating variation with d_j. Spectral analysis shows that the photocurrent is available for wavelengths of 360 to 730 nm, among which photons of 400 to 650 nm provide major contributions. The photocurrent was in the range of 1×10^8 to 7×10^8 $Am^{-2} nm^{-1}$ for an irradiance of 1000 W/m². The device, operated with a negative terminal voltage, was found to be useful as a photodiode for light sensing. The results of this study are consistent with those of the previous reports. This work produces a better prediction of OSC performance because of improved analytical calculations using spatial recombination coefficients, space-and wavelength-dependent excitons, and improved dissociation probability incorporating Gaussian distribution, altogether. Hence, this work may provide clues for the better design of organic solar cells.

APPENDIX A

$$t_j^+ = \frac{1}{S'_{11} + S'_{12} r'' e^{i2\xi_j d_j}}$$

$$r'' = \frac{S''_{21}}{S''_{11}}$$

$$\xi_j = \frac{2\pi \tilde{\eta}_j}{\lambda}$$

$$\tilde{\eta}_j = (\eta_j + i\kappa_j)$$

$\eta_j = $ refractive index of active layer material

$\kappa_j = $ extinction coefficient of active layer material

$d_j = $ active layer thickness

$$H(x) = \left[e^{-\alpha_j x} + L e^{\alpha_j x} + M \cos(N - Rx) \right]$$

$$\alpha_j = \frac{4\pi \kappa_j}{\lambda} = \text{absorption coefficient of active layer}$$

$$L = \rho''^2 e^{-2\alpha_j d_j}$$

$$M = 2\rho'' e^{-\alpha_j d_j}$$

$$N = \left(\frac{4\pi \eta_j d_j}{\lambda} + \delta'' \right)$$

$$R = \frac{4\pi \eta_j}{\lambda}$$

$$\rho'' = |r''|$$

$$\delta'' = \angle r''$$

APPENDIX B

$$D = D_p + D_n$$

$$D_p = \frac{k_B T \mu_p}{q} = \text{hole diffusion coefficient}$$

$$D_n = \frac{k_B T \mu_n}{q} = \text{electron diffusion coefficient}$$

k_B = Boltzmann's constant

T = Temperature in Kelvin

μ_p (μ_n) = mobility of holes (electrons)

q = electronic charge value

$r_c = \dfrac{q^2}{4\pi\varepsilon k_B T}$ = Onsager radius

$\varepsilon = \varepsilon_r \varepsilon_0$ = electric permittivity

ε_r = relative permittivity or dielectric constant

ε_0 = air (vacuum) permittivity

$b = \dfrac{|q^3||F|}{8\pi\varepsilon k_B^2 T^2}$ = a parameter related to the field

$|F|$ = magnitude of the electric field across active layer

APPENDIX C

$$a_1 = \frac{-qF}{k_B T}$$

$$a_2 = \frac{-qr_m}{k_B T \mu}$$

$$a_3 = \frac{-q}{k_B T \mu}$$

$$\omega_1 = \frac{-a_1 + \sqrt{a_1^2 - 4a_2}}{2}$$

$$\omega_2 = \frac{-a_1 - \sqrt{a_1^2 - 4a_2}}{2}$$

$$a_4 = \frac{a_3 K}{\left(\alpha_j^2 - a_1\alpha_j + a_2\right)}$$

$$a_5 = \frac{a_3 KL}{\left(\alpha_j^2 + a_1\alpha_j + a_2\right)}$$

$$a_6 = \frac{a_3 KM\left(a_2 - R^2\right)}{\left(a_2 - R^2\right)^2 + a_1^2 R^2}$$

$$a_7 = \frac{-a_3 KMa_1 R}{\left(a_2 - R^2\right)^2 + a_1^2 R^2}$$

APPENDIX D

The number of holes is related to the energy difference between the Fermi level (E_f) and valence band level (E_v). Theoretically, [13], [41] the hole concentration (p) can be calculated as, $p = N_v e^{-(E_f - E_v)/k_B T} = N_v e^{-E_{fv}/E_t}$; where N_v = effective density of states in the valence band, $E_{fv} = (E_f - E_v)$, and $E_t = k_B T$ = thermal energy.

Theoretically, [13], [41] the electron concentration (n) can be calculated as, $n = N_c e^{-(E_c - E_f)/k_B T} = N_c e^{-E_{cf}/E_t}$; where N_c = the effective density of states in the conduction band, E_c = conduction band energy level, $E_{cf} = (E_c - E_f)$.

In general, for any charge carrier, we may write $Q = N_s e^{-E_d/E_t}$; where Q = concentration of charge carriers (holes or electrons), N_s = density of states (N_v for holes, N_c for electrons), E_d = energy difference (E_{fv} for holes, E_{cf} for electrons). E_d and E_t must be of the same unit.

At $x = 0$, if $E_d = E_{d0}$ then the concentration of charge carriers is $[Q]_{x=0} = N_s e^{-E_{d0}/E_t}$; where $E_{d0} = E_{d0p}$ for holes and E_{d0n} for electrons, as shown in Fig. 2(b). By applying this boundary value of Q in Eq. (29), we obtain

$$N_s e^{-\frac{E_{d0}}{E_t}} = [Q_{dark}]_{x=0} + \int_{\lambda_1}^{\lambda_2} [Q_{ph}]_{x=0}\, d\lambda \qquad (D1)$$

At the boundary position at $x = 0$, the charge carrier concentration depends on the energy difference E_{d0}, which does not depend on the incident light; that is, the boundary charge carrier does not depend on light (λ). Therefore, λ-related part at RHS of Eq. (D1) should be zero; on the other hand, the constant parts on the two sides of Eq. (D1) should be equal.

$$\text{Constant part}: [Q_{dark}]_{x=0} = N_s e^{-\frac{E_{d0}}{E_t}}$$

$$\Rightarrow A_1 + A_2 = N_s e^{-\frac{E_{d0}}{E_t}} \qquad (D2)$$

$$\lambda \text{ Related part}: \int_{\lambda_1}^{\lambda_2} [Q_{ph}]_{x=0}\, d\lambda = 0$$

Differentiating the above equation with respect to λ

$$A_3 + A_4 = a_8 \qquad (D3)$$

where $a_8 = -\{a_4 + a_5 + a_6 \cos(N) + a_7 \sin(N)\}$

At $x = d_j$, if $E_d = E_{dj}$ then the concentration of charge carriers is $[Q]_{x=d_j} = N_s e^{-E_{dj}/E_t}$; where $E_{dj} = E_{djp}$ for holes and E_{djn} for electrons, as shown in Fig. 2(b). By applying this boundary value of Q in Eq. (29), we obtain

$$N_s e^{-\frac{E_{dj}}{E_t}} = [Q_{dark}]_{x=d_j} + \int_{\lambda_1}^{\lambda_2} [Q_{ph}]_{x=d_j}\, d\lambda \qquad (D4)$$

$$\text{Constant part}: [Q_{dark}]_{x=d_j} = N_s e^{-\frac{E_{dj}}{E_t}}$$

$$\Rightarrow A_1 e^{\omega_1 d_j} + A_2 e^{\omega_2 d_j} = N_s e^{-\frac{E_{dj}}{E_t}} \qquad (D5)$$

$$\lambda \text{ Related part}: \int_{\lambda_1}^{\lambda_2} [Q_{ph}]_{x=d_j}\, d\lambda = 0$$

Differentiating the above equation with respect to λ

$$A_3 e^{\omega_1 d_j} + A_4 e^{\omega_2 d_j} = a_9 \qquad (D6)$$

where

$$a_9 = -\{a_4 e^{-\alpha_j d_j} + a_5 e^{\alpha_j d_j} + a_6 \cos(N - Rd_j) + a_7 \sin(N - Rd_j)\}$$

By solving Eqs. (D2) and (D5), we may find A_1 and A_2 as follows:

$$A_1 = \frac{N_s}{A}\left[e^{\left(-\frac{E_{d0}}{E_t} + \omega_2 d_j\right)} - e^{-\frac{E_{dj}}{E_t}}\right]$$

$$A_2 = -\frac{N_s}{A}\left[e^{\left(-\frac{E_{d0}}{E_t} + \omega_1 d_j\right)} - e^{-\frac{E_{dj}}{E_t}}\right]$$

where $A = \left[e^{\omega_2 d_j} - e^{\omega_1 d_j}\right]$

Similarly, by solving Eqs. (D3) and (D6), we may find A_3 and A_4 as follows:

$$A_3 = \frac{1}{A}\left[a_8 e^{\omega_2 d_j} - a_9\right]$$

$$A_4 = -\frac{1}{A}\left[a_8 e^{\omega_1 d_j} - a_9\right]$$

APPENDIX E

$$A_{11} = \mu A_1 \left(qF - k_B T \omega_1 \right)$$

$$A_{12} = \mu A_2 \left(qF - k_B T \omega_2 \right)$$

$$A_{21} = \mu A_3 \left(qF - k_B T \omega_1 \right)$$

$$A_{22} = \mu A_4 \left(qF - k_B T \omega_2 \right)$$

$$A_{23} = \mu a_4 \left(qF + k_B T \alpha_j \right)$$

$$A_{24} = \mu a_5 \left(qF - k_B T \alpha_j \right)$$

$$A_{25} = \mu \left(qF a_6 + k_B T R b_7 \right)$$

$$A_{26} = \mu \left(qF a_7 - k_B T R b_6 \right)$$

ACKNOWLEDGMENT

REFERENCES

[1] N. Marinova, S. Valero, and J. L. Delgado, "Organic and perovskite solar cells: Working principles, materials and interfaces," *J. Colloid Interface Sci.*, vol. 488, pp. 373–389, Feb. 2017.

[2] B. Ratier, J.-M. Nunzi, M. Aldissi, T. M. Kraft, and E. Buncel, "Organic solar cell materials and active layer designs-improvements with carbon nanotubes: A review," *Polym. Int.*, vol. 61, no. 3, pp. 342–354, Mar. 2012.

[3] T. F. O'Connor, A. V. Zaretski, S. Savagatrup, A. D. Printz, C. D. Wilkes, M. I. Diaz, E. J. Sawyer, and D. J. Lipomi, "Wearable organic solar cells with high cyclic bending stability: Materials selection criteria," *Sol. Energy Mater. Sol. Cells*, vol. 144, pp. 438–444, Jan. 2016.

[4] O. K. Kwon, M. A. Uddin, J.-H. Park, S. K. Park, T. L. Nguyen, H. Y. Woo, and S. Y. Park, "A high efficiency nonfullerene organic solar cell with optimized crystalline organizations," *Adv. Mater.*, vol. 28, no. 5, pp. 910–916, Feb. 2016.

[5] G. Li, L. Liu, F. Wei, S. Xia, and X. Qian, "Recent progress in modeling, simulation, and optimization of polymer solar cells," *IEEE J. Photovolt.*, vol. 2, no. 3, pp. 320–340, Jul. 2012.

[6] W. Ma, C. Yang, X. Gong, K. Lee, and A. J. Heeger, "Thermally stable, efficient polymer solar cells with nanoscale control of the interpenetrating network morphology," *Adv. Funct. Mater.*, vol. 15, no. 10, pp. 1617–1622, Oct. 2005.

[7] G. Li, V. Shrotriya, J. Huang, Y. Yao, T. Moriarty, K. Emery, and Y. Yang, "High-efficiency solution processable polymer photovoltaic cells by self-organization of polymer blends," *Nature Mater.*, vol. 4, no. 11, pp. 864–868, Oct. 2005.

[8] M. A. Green and ChemViews, "Solar cell efficiency tables," *ChemViews*, vol. 20, pp. 12–20, Oct. 2012.

[9] R. Hausermann, E. Knapp, M. Moos, N. A. Reinke, T. Flatz, and B. Ruhstaller, "Coupled optoelectronic simulation of organic bulk-heterojunction solar cells: Parameter extraction and sensitivity analysis," *J. Appl. Phys.*, vol. 106, no. 10, Nov. 2009, Art. no. 104507.

[10] L. J. A. Koster, E. C. P. Smits, V. D. Mihailetchi, and P. W. M. Blom, "Device model for the operation of polymer/fullerene bulk heterojunction solar cells," *Phys. Rev. B, Condens. Matter*, vol. 72, no. 8, Aug. 2005, Art. no. 085205.

[11] F. Monestier, J.-J. Simon, P. Torchio, L. Escoubas, F. Flory, S. Bailly, R. de Bettignies, S. Guillerez, and C. Defranoux, "Modeling the short-circuit current density of polymer solar cells based on P3HT: PCBM blend," *Sol. Energy Mater. Sol. Cells*, vol. 91, no. 5, pp. 405–410, Mar. 2007.

[12] D. W. Sievers, V. Shrotriya, and Y. Yang, "Modeling optical effects and thickness dependent current in polymer bulk-heterojunction solar cells," *J. Appl. Phys.*, vol. 100, May 2006, Art. no. 114509.

[13] P. Kumar, S. C. Jain, V. Kumar, S. Chand, and R. P. Tandon, "A model for the *J* − *V* characteristics of P3HT:PCBM solar cells," *J. Appl. Phys.*, vol. 105, May 2009, Art. no. 104507.

[14] R. A. Marsh, C. R. McNeill, A. Abrusci, A. R. Campbell, and R. H. Friend, "A unified description of current–voltage characteristics in organic and hybrid photovoltaics under low light intensity," *Nano Lett.*, vol. 8, no. 5, pp. 1393–1398, May 2008.

[15] S. Altazin, R. Clerc, R. Gwoziecki, G. Pananakakis, G. Ghibaudo, and C. Serbutoviez, "Analytical modeling of organic solar cells and photodiodes," *Appl. Phys. Lett.*, vol. 99, Oct. 2011, Art. no. 143301.

[16] L. Torto, A. Cester, N. Wrachien, M. Seri, and M. Muccini, "Drift-diffusion and analytical modeling of the recombination mechanisms in organic solar cells: Effect of the nonconstant charge distribution inside the active layer," *IEEE J. Photovolt.*, vol. 8, no. 6, pp. 1677–1684, Nov. 2018.

[17] D. E. Aspnes, "Optical properties of thin films," *Thin Solid Films*, vol. 89, no. 3, pp. 249–262, Mar. 1982.

[18] L. A. A. Pettersson, L. S. Roman, and O. Inganäs, "Modeling photocurrent action spectra of photovoltaic devices based on organic thin films," *J. Appl. Phys.*, vol. 86, no. 1, pp. 487–496, 1999.

[19] M. M. Chowdhury and M. K. Alam, "An analytical model for bulk heterojunction organic solar cells using a new empirical expression of space dependent photocarrier generation," *Sol. Energy*, vol. 126, pp. 64–72, Mar. 2016.

[20] M. S. S. Rahman and M. K. Alam, "Effect of angle of incidence on the performance of bulk heterojunction organic solar cells: A unified optoelectronic analytical framework," *AIP Adv.*, vol. 7, May 2017, Art. no. 065101.

[21] M. Islam, S. Wahid, M. M. Chowdhury, F. Hakim, and M. K. Alam, "Effect of spatial distribution of generation rate on bulk heterojunction organic solar cell performance: A novel semi-analytical approach," *Organic Electron.*, vol. 46, pp. 226–241, Jul. 2017.

[22] S. M. Arnab and M. Z. Kabir, "An analytical model for analyzing the current-voltage characteristics of bulk heterojunction organic solar cells," *J. Appl. Phys.*, vol. 115, 2014, Art. no. 034504.

[23] L. Liu and G. Li, "Investigation of recombination loss in organic solar cells by simulating intensity-dependent current–voltage measurements," *Sol. Energy Mater. Sol. Cells*, vol. 95, no. 9, pp. 2557–2563, Sep. 2011.

[24] L. Onsager, "Initial recombination of ions," *Phys. Rev.*, vol. 54, no. 8, pp. 554–557, Oct. 1938.

[25] C. L. Braun, "Electric field assisted dissociation of charge transfer states as a mechanism of photocarrier production," *J. Chem. Phys.*, vol. 80, no. 9, pp. 4157–4161, May 1984.

[26] M. S. Islam, "Analytical modeling of organic solar cells including monomolecular recombination and carrier generation calculated by optical transfer matrix method," *Organic Electron.*, vol. 41, pp. 143–156, Feb. 2017.

[27] M. M. Chowdhury and M. K. Alam, "A physics-based analytical model for bulk heterojunction organic solar cells incorporating monomolecular recombination mechanism," *Current Appl. Phys.*, vol. 14, no. 3, pp. 340–344, Mar. 2014.

[28] A. E. Iverson and D. L. Smith, "Mathematical modeling of photoconductor transient response," *IEEE Trans. Electron Devices*, vol. ED-34, no. 10, pp. 2098–2107, Oct. 1987.

[29] S. M. Arnab and M. Z. Kabir, "Modeling of the effects of charge transport on voltage-dependent photocurrent in ultrathin CdTe solar cells," *J. Vac. Sci. Technol. A, Vac. Surf. Films*, vol. 31, Oct. 2013, Art. no. 061201.

[30] M. M. Chowdhury and M. K. Alam, "An optoelectronic analytical model for bulk heterojunction organic solar cells incorporating position and wavelength dependent carrier generation," *Sol. Energy Mater. Sol. Cells*, vol. 132, pp. 107–117, Jan. 2015.

[31] M. S. Islam, "In-depth analysis of organic solar cells using transport equation and optical transfer matrix method with detailed analytical derivations," *Energies*, vol. 14, pp. 735-1–735-28, 2021.

[32] M. Wojcik and M. Tachiya, "Accuracies of the empirical theories of the escape probability based on Eigen model and Braun model compared with the exact extension of Onsager theory," *J. Chem. Phys.*, vol. 130, May May 2009, Art. no. 104107.

[33] M. Hilczer and M. Tachiya, "Unified theory of geminate and bulk electron-hole recombination in organic solar cells," *J. Phys. Chem. C*, vol. 114, no. 14, pp. 6808–6813, Apr. 2010.

[34] L. Onsager, "Deviations from Ohm's law in weak electrolytes," *J. Chem. Phys.*, vol. 2, no. 9, pp. 599–615, Sep. 1934.

[35] V. A. Trukhanov, V. V. Bruevich, and D. Y. Paraschuk, "Effect of doping on performance of organic solar cells," *Phys. Rev. B, Condens. Matter*, vol. 84, no. 20, Nov. 2011, Art. no. 205318.

[36] Y. M. Nam, J. Huh, and W. H. Jo, "Optimization of thickness and morphology of active layer for high performance of bulk-heterojunction organic solar cells," *Sol. Energy Mater. Sol. Cells*, vol. 94, pp. 1118–1124, Jun. 2010.

[37] G. Li and L. Liu, "Carbon nanotubes for organic solar cells," *IEEE Nanotechnol. Mag.*, vol. 5, no. 3, pp. 18–24, Sep. 2011.

[38] V. Shrotriya, G. Li, Y. Yao, C. W. Chu, and Y. Yang, "Transition metal oxides as the buffer layer for polymer photovoltaic cells," *Appl. Phys. Lett.*, vol. 88, May 2006, Art. no. 073508.

[39] C. W. Liang, W. F. Su, and L. Wang, "Enhancing the photocurrent in poly(3-hexylthiophene)/[6,6]-phenyl C$_{61}$ butyric acid methyl ester bulk heterojunction solar cells by using poly(3-hexylthiophene) as a buffer layer," *Appl. Phys. Lett.*, vol. 95, May 2009, Art. no. 133303.

[40] D. S. Ginley and D. Cahen, *Fundamentals of Materials for Energy and Environmental Sustainability*, Cambridge, U.K.: Cambridge Univ. Press, 2011.

[41] S. M. Sze, *Physics of Semiconductor Devices*. New York, NY, USA: Wiley, 1981.

[42] American Society for Testing and Materials. *Solar Spectral Irradiance: Air Mass 1.5*. Accessed: Mar. 15, 2020. [Online]. Available: http://rredc.nrel.gov/solar/spectra/am1.5/

[43] H. M. Rad, F. Zhu, and J. Singh, "Profiling exciton generation and recombination in conventional and inverted bulk heterojunction organic solar cells," *J. Appl. Phys.*, vol. 124, Aug. 2018, Art. no. 083103.

[44] K. S. Nalwa, H. K. Kodali, B. Ganapathysubramanian, and S. Chaudhary, "Dependence of recombination mechanisms and strength on processing conditions in polymer solar cells," *Appl. Phys. Lett.*, vol. 99, Dec. 2011, Art. no. 263301.

[45] M. Saleheen, S. M. Arnab, and M. Z. Kabir, "Analytical Model for Voltage-dependent photo and dark currents in bulk heterojunction organic solar cells," *Energies*, vol. 9, pp. 1–14, Jun. 2016.

[46] J. J. Khanam and S. Y. Foo, "Modeling of high-efficiency multi-junction polymer and hybrid solar cells to absorb infrared light," *Polym.*, vol. 11, pp. 1–16, Feb. 2019.

[47] S. Yang, X. Sun, Y. Zhang, G. Li, X. Zhao, X. Li, and G. Fu, "Enhancing the efficiency of polymer solar cells by modifying buffer layer with N, N-dimethylacetamide," *Int. J. Photoenergy*, vol. 2014, Oct. 2014, Art. no. 854749.

[48] K. Yoshida, T. Oku, A. Suzuki, T. Akiyama, and Y. Yamasaki, "Fabrication and characterization of PCBM: P3HT bulk heterojunction solar cells doped with germanium phthalocyanine or germanium naphthalocyanine," *Mater. Sci. Appl.*, vol. 4, no. 4, 2013, Art. no. 30171.

[49] E. J. Lee, M. H. Choi, and D. K. Moon, "Enhanced photovoltaic properties of bulk heterojunction organic photovoltaic devices by an addition of a low band gap conjugated polymer," *Materials*, vol. 9, p. 996, Dec. 2016.

[50] M. Ikram, N. A. Niaz, N. R. Khalid, M. Ramzan, M. Imran, and S. Ali, "Tetra blended based hybrid bulk heterojunction solar cells," *J. Ovonic Res.*, vol. 10, no. 6, pp. 257–263, Nov. 2014.

MD. SHOFIQUL ISLAM received the B.Sc. and M.Sc. degrees in electrical and electronic engineering from Bangladesh University of Engineering and Technology, Bangladesh, in 1999 and 2002, respectively, and the Ph.D. degree in electronic and information engineering from Toyohashi University of Technology, Japan, in 2007.

He has work experience in Si crystal growth and fabricating electronic devices, sensors, and MEMs structures. He is currently working as an Associate Professor with the Department of Electrical and Computer Engineering, King Abdulaziz University, Saudi Arabia. His current research interests include modeling and simulation of electronic devices, sensors, solar cells (organic and Si-based), and design and analysis of special shaped devices for sensor applications.

Dr. Islam received the Best Paper Award in Asia–Pacific Conference of Transducers and Micro-Nano Technology (APCOT), Singapore.

● ● ●